DOI 10.1007/s00231-014-1391-4

Scaling heat and mass flow through porous media during pyrolysis

Julien Maes · Ann H. Muggeridge · Matthew D. Jackson · Michel Quintard · Alexandre Lapene

Abstract The modelling of heat and mass flow through porous media in the presence of pyrolysis is complex because various physical and chemical phenomena need to be represented. In addition to the transport of heat by conduction and convection, and the change of properties with varying pressure and temperature, these processes involve transport of mass by convection, evaporation, condensation and pyrolysis chemical reactions. Examples of such processes include pyrolysis of wood, thermal decomposition of polymer composite and in situ upgrading of heavy oil and oil shale. The behaviours of these systems are difficult to predict as relatively small changes in the material composition can significantly change the thermophysical properties. Scaling reduces the number of parameters in the problem statement and quantifies the relative importance of the various dimensional parameters such as permeability, thermal conduction and reaction constants. This paper uses inspectional analysis to determine the minimum number of dimensionless scaling groups that describe the decomposition of a solid porous material into a gas in one dimension. Experimental design is then used to rank these scaling groups in terms of their importance in describing the outcome of two example processes: the thermal decomposition of heat shields formed from polymer composites and the in situ upgrading of heavy oils and oil shales. A sensitivity analysis is used to divide these groups into three sets (primary, secondary and insignificant), thus identifying the combinations of solid and fluid properties that have the most impact on the performance of the different processes.

J. Maes (✉) · A. H. Muggeridge · M. D. Jackson
Department of Earth Science and Engineering, Imperial College London, London, UK
e-mail: j.maes12@imperial.ac.uk

M. Quintard
INPT, UPS , IMFT (Institut de Mécanique des Fluides de Toulouse), Université de Toulouse, Allée Camille Soula, 31400 Toulouse, France

M. Quintard
CNRS, IMFT, 31400 Toulouse, France

A. Lapene
Total CSTJF, Avenue Larribau, 64000 Pau, France

List of symbols

Roman symbols

A	Frequency factor (s^{-1})
E_a	Activation energy (J/mol)
F	Fraction of remaining reactant
h	Specific enthalpy (J/kg)
K	Rock permeability (m^2)
L	Domain length (m)
M	Molecular weight (kg/kmol)
P	Pressure (Pa)
q	Energy flow by conduction (W/m^2)
R	Universal gas constant (8.314 J/mol/K)
T	Temperature (K)
t	Time (s)
τ	Time scale of heat conduction in porous media (s)

Subscripts

0	Initial value
v	Velocity (m/s)
x	One dimensional coordinate (m)

Greek symbols

Δh_r	Reaction enthalpy (J/kg)
ΔT	Temperature scale $\Delta T = T_i - T_0$ (K)
ϵ	Emissivity
γ	Specific heat capacity (J/kg K)
κ	Thermal conductivity (W/m K)
μ	Viscosity (Pa s)
ϕ	rock porosity (no unit)
ρ	Mass density (kg/m^3)
σ	Stefan–Boltzmann constant (5.67×10^{-8} W/m^2/K^4)
f	Final value
g	Gas
i	Incident heat value
s	Solid

1 Introduction

The thermal decomposition of porous solids by pyrolysis involves a range of processes including heat and mass transport, phase behaviour and chemical reactions. There are numerous applications of pyrolysis; examples include thermal decomposition of polymer composites when used as heat shields during spacecraft re-entry or for rocket nozzle protection [2, 13], wood and biomass pyrolysis for heat generation [16, 20, 31], or in situ upgrading of oil shale or heavy oil [5, 18]. Oil shale is one of the most promising unconventional sources of energy in the world, with large deposits situated in almost all the continents. In situ upgrading is a process that uses heat to decompose the solid kerogen through a series of chemical reactions into liquid and gas hydrocarbons.

In all these processes, an external energy source, such as electrical heaters or gas burners, heats one edge of the porous solid. This heat propagates into the solid by conduction. Once the solid reaches a sufficiently high temperature it decomposes into liquid and/or gas by pyrolysis. Typically this will occur initially in a zone near the energy source. This reaction zone then propagates into the solid following the heat front. During the initial stages of pyrolysis the reaction products are trapped in pores within the solid, resulting in an increase of pressure in the heated domain; however, as more of the solid decomposes, these pores become interconnected and the liquid and/or gas can flow away from the reaction zone. This fluid transport also enables further heat transfer via convection.

It is challenging to predict the outcome of thermal decomposition in porous media because it depends upon a large number of physical parameters, the values of which are often uncertain e.g., the reaction constants and the temperature dependence of the material properties [8, 10]. In addition, the relative importance of these parameters depends upon the application. Numerical simulation can be used but needs to be calibrated and validated by reference to laboratory studies. In most cases these laboratory studies are performed on different length scales and under different conditions from the planned application. This means they cannot be used directly in designing that application [13].

Analysis using dimensionless numbers can provide useful insight into the relative importance of different parameters and processes, especially if combined with experimental design, which allows quantification of the impact of the parameters with a minimal number of computation. Dimensionless numbers are often used to scale laboratory results to the application length scale and conditions, and may be developed using techniques such as dimensionless analysis (DA) [26] and inspectional analysis (IA) [27]. Ranking the different parameters controlling a given thermal decomposition application enables experimental programmes to be focussed on acquiring the relevant data with the appropriate accuracy. It can also enable better design of that application and, potentially, the development of more robust and efficient numerical simulation tools.

In this paper, we determine the set of dimensionless numbers required to analyse the thermal decomposition of solid charring materials and identify which of those numbers are most important for two very different applications: the thermal decomposition of polymer composites for heat shielding and the thermal conversion of oil shale into non-reactive gas. The dimensionless numbers were derived using a mathematical model of these two systems, which are identical apart from boundary conditions. The relative importance of the dimensionless numbers was determined by performing a sensitivity analysis using a numerical model written specifically for this investigation. The model and boundary conditions for the thermal degradation of polymer is identical to that of Henderson and Wiecek [13]. This allowed us to validate our model by comparison with the experimental results described in their paper.

2 One-dimensional models

The first application we model is the thermal decomposition of polymer composite when used for heat shielding during spacecraft re-entry or for rocket nozzle protection. Figure 1a illustrates our conceptual model of this process. This is based on the model of Henderson and Wiecek [13] where the gas can flow out of the lateral boundaries. Note that a different model could consider an impervious right boundary condition. In this case the results would be modified but not the methodology. Radiative heat flux causes the thermal decomposition and is represented by the incident heat flux on the left end of the domain. The material can exchange heat at both ends by radiation. The

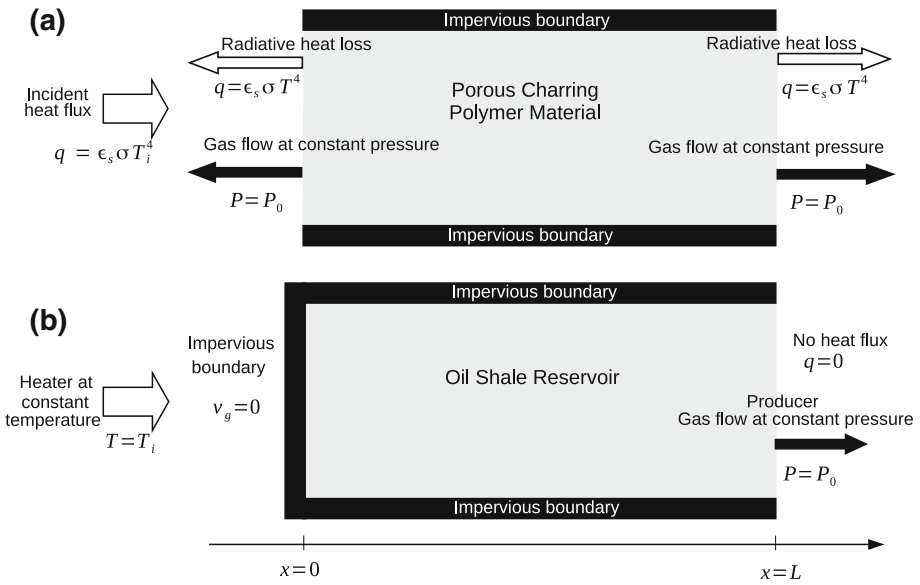

Fig. 1 Model for thermal decomposition of polymer composite as represented in Henderson and Wiecek experiment (**a**) and thermal conversion of oil shale into non-reactive gas (**b**). The two models only differ in their boundary conditions

boundary pressure on both ends is equal to the initial pressure P_0.

The second application we investigate is the thermal conversion of oil shale into non-reactive gas as a simplified model for in situ upgrading by subsurface pyrolysis for the recovery of oil shale. In this process, the reservoir is exposed to an external energy source such as electrical heaters or gas burners. The in situ upgrading process generally uses tightly spaced electrical heaters in boreholes to slowly and uniformly heat the formation by thermal conduction to the conversion temperature of about 350 °C [7]. The gas created by the decomposition of the oil shale flows into the borehole of a producing well.

A mathematical model for this application was developed by Fan et al. [5]. We observed that the chemical reactions and the fluid and material behaviors can be described using the same model as Henderson and Wiecek's thermal decomposition of polymer composite [13]. The two processes only differ in their geometry, boundary conditions and fluid and material properties. Thus it is sensible to identify the two processes in the same study.

In this paper, we consider a one-dimensional oil shale reservoir (Fig. 1b). The domain is bounded by the heater boreholes on the left end and the well producer on the right end. To define the boundary conditions, we assume a constant temperature T_i around the heater. On the left end of the domain, we assume no mass flow. On the right end of the domain, the well produces at constant pressure and, due to the symmetry of the problem, we assume no heat transfer by conduction around the producer.

For both models, the following assumptions are made:

1. The solid decomposes into a non-reactive gas with a single reaction mechanism (following [13, 16]). Further primary pyrolysis reactions do occur but for simplicity are ignored.
2. The decomposition gas behaves ideally.
3. Gas flows are described by Darcy's law.
4. The gas viscosity has a linear dependence on temperature.
5. Porosity and permeability are linear functions of the solid fraction remaining as the reaction progresses.
6. Local thermal equilibrium (LTE) exists between the solid and the decomposition gas.
7. Thermal expansion of the solid is negligible.
8. Solid and gas heat capacities and thermal conductivities are constant.

Assumptions 1–5 have been used previously by Kansa et al. [16] and Henderson and Wiecek [13]. Florio et al. [6] used analytical methods to study the validity of assumption 6 during the thermal decomposition of a particular glass filled polymer composite. They found that the gas and solid phases were not always in LTE but this affected mainly the mechanical behaviour of the composite rather than the heat and mass transfer. Puiroux et al. [24] also found that the main impact was on the maximum pressure reached and hence the mechanical response of the material although they did observe a small effect on the position of the pyrolysis front. Our study is focussed primarily on the scaling of heat and mass transport rather than the mechanical behaviour (hence assumption 7) so assumption 6 simplifies our analysis without significantly affecting our predictions. Assumptions 7 and 8 are discussed in the next section.

The models are described by the following equations. The rate of decomposition follows an Arrhenius law of order n:

$$\frac{1}{\rho_{s,0}-\rho_{s,f}}\frac{\partial \rho_s}{\partial t} = -A\left(\frac{\rho_s-\rho_{s,f}}{\rho_{s,0}-\rho_{s,f}}\right)^n \exp\left(-\frac{E_a}{RT}\right) \tag{1}$$

where the terms with subscript 0 are initial values and terms with subscript f are final values (when all reactant has decomposed). Note that we decided to use a more common formulation for the rate of decomposition [8] than Henderson and Wiecek's where the pre-exponential factor A_{HW} is applied as follow:

$$\frac{1}{\rho_{s,0}}\frac{\partial \rho_s}{\partial t} = -A_{HW}\left(\frac{\rho_s-\rho_{s,f}}{\rho_{s,0}}\right)^n \exp\left(-\frac{E_a}{RT}\right) \tag{2}$$

The pre-exponential factor used in Eq. (1) is obtained from A_{HW}:

$$A = A_{HW}\left(1-\frac{\rho_{s,f}}{\rho_{s,0}}\right)^{n-1} \tag{3}$$

The porosity and permeability of the solid material are given by:

$$\phi = \phi_0 F + \phi_f(1-F) \tag{4}$$

$$K = K_0 F + K_f(1-F) \tag{5}$$

where

$$F = \frac{\rho_s-\rho_{s,f}}{\rho_{s,0}-\rho_{s,f}} \tag{6}$$

The total mass conservation equation reads:

$$\frac{\partial \phi \rho_g}{\partial t} = -\frac{\partial \rho_g v_g}{\partial x} - \frac{\partial \rho_s}{\partial t} \tag{7}$$

The left-hand side of Eq. (7) is the rate of mass accumulation of gas in the pores. The first term on the right represents the rate of change of the mass flow and the last term the rate of gas generation by pyrolysis. The ideal gas equation of state is used for gas density:

$$\rho_g = \frac{M_g P}{RT} \tag{8}$$

The velocity of the gas is given by Darcy's law:

$$v_g = -\frac{K}{\mu_g}\frac{\partial P}{\partial x} \tag{9}$$

with the gas viscosity given by:

$$\mu_g = \mu_{g,0} + \frac{\partial \mu_g}{\partial T}(T-T_0) \tag{10}$$

Given local thermal equilibrium between the solid and the decomposition gas, then the energy conservation equation is:

$$\frac{\partial}{\partial t}\left(\rho_s h_s + \phi \rho_g h_g\right) = -\frac{\partial}{\partial x}\left(\rho_g v_g h_g\right) - \frac{\partial q}{\partial x} - \Delta h_r \frac{\partial \rho_s}{\partial t} \tag{11}$$

where the enthalpy of the solid and the enthalpy of the gas are given by:

$$h_i = \gamma_i (T-T_0), \quad i = s, g \tag{12}$$

The first term in Eq. (11) is the rate of energy accumulation in the domain; the second term represents the rate of energy transferred by convection; the third term represents the rate of energy transferred by conduction; the last term accounts for energy consumption or generation by chemical reactions. This equation is modified by expanding the accumulation and convection terms and then substituting in the mass conservation equation (7), to yield:

$$\left(\rho_s \gamma_s + \phi \rho_g \gamma_g\right)\frac{\partial T}{\partial t} = -\rho_g v_g \gamma_g \frac{\partial T}{\partial x} - \frac{\partial q}{\partial x} - \left(\Delta h_{r0} + h_s - h_g\right)\frac{\partial \rho_s}{\partial t} \tag{13}$$

Finally, the heat flow by conduction q is given by Fourier's law:

$$q = -\left((1-\phi)\kappa_s + \phi \kappa_g\right)\frac{\partial T}{\partial x} \tag{14}$$

In Eq. 14, we have adopted for convenience a simple estimate of the effective thermal conductivity which depends on the volume fraction of the solid and gas in the material. This approximation has been previously used [3]. More complex expressions would not fundamentally change the analysis. Equations (1), (7), (9), (13) and (14) form a set of coupled non-linear equations to be solved simultaneously for ρ_s, P, T, v_g and q.

For the heat flow boundary conditions, we assume constant flux with heat loss by radiation, or constant temperature. For the thermal conversion of oil shale, the heating temperature T_i is defined as the temperature of the heater well bore, while for the thermal decomposition of polymer composite, T_i is defined as the effective temperature of the radiative source. This gives:

$$\begin{aligned} &\text{at} \quad x = 0 \quad \forall t \\ &q = \epsilon_s \sigma\left(T_i^4 - T^4\right) \quad \text{or} \quad T = T_i \\ &\text{at} \quad x = L \quad \forall t \\ &q = -\epsilon_s \sigma T^4 \quad \text{or} \quad q = 0 \end{aligned} \tag{15}$$

For the mass flow boundary conditions, we assume constant pressure P_0 or no mass flux. This gives:

$$\begin{aligned} &\text{at} \quad x = 0 \quad \forall t \\ &P = P_0 \quad \text{or} \quad v_g = 0 \\ &\text{at} \quad x = L \quad \forall t \\ &P = P_0 \end{aligned} \tag{16}$$

Finally, we apply the following initial conditions:

$$\begin{aligned} &\rho_s = \rho_{s,0} \\ &T = T_0 \quad \text{at} \quad t = 0 \quad \forall x \\ &P = P_0 \end{aligned} \tag{17}$$

To solve the system of equations, a MATLAB simulator using the control volume method [23] was developed. We used an implicit solution technique with the Newton–Raphson algorithm to handle non-linearities [17].

3 Validation of the mathematical model

We validated our mathematical model first by comparing its output with analytical solutions for the trivial cases of very short time (heat conduction and no reaction) and very long times (after pyrolysis is finished). Having obtained good agreement for these cases, we then compared its predictions with the experimental data for the thermal decomposition of a polymer composite obtained by Henderson and Wiecek [13]. As noted previously, the same mathematical model describes polymer degradation and in situ upgrading of oil shale, the only difference between the two systems is in the boundary conditions. Henderson and Wiecek developed a mathematical model for one dimensional heat transfer in a polymer matrix composite during pyrolysis and performed laboratory experiments to validate their model. The material used in their experiments consisted of a basic phenolic resin and was chosen because it displays typical decomposition/expansion behaviour for glass-filled composites and is used in a large number of high-temperature thermal protection applications [6, 13]. The experimental study was conducted using a 3 cm thick slab subjected to a pure radiant heat flux. The pressure at both ends, as well as the initial pressure, was 1×10^5 Pa and the initial temperature was 24 °C. The gas and material properties used in their simulations were obtained after a careful literature review of [10–13].

In our study, we choose to neglect the thermal expansion of the solid (assumption 7). The maximum solid elongation reported by Henderson and Wiecek [13] was <20 %. Therefore, we assume that the expansion has little impact on the heat propagation, the solid decomposition and the gas flow. In order to simplify the model, the thermal properties of the solid and gas (heat capacity, thermal conductivity, emissivity) are taken as constant and so do not change with temperature and the fraction of remaining reactant (assumption 8). We note that Henderson and Wiecek [13] allowed the thermal properties to change with temperature in their study; however, we choose values for these thermal properties so that the solid temperature obtained in our simulation and the solid temperature reported in Henderson and Wiecek [13] are similar. The solid and gas properties, along with the initial and boundary conditions that we use in our simulation are summarized in Table 1.

Table 1 Summary of parameters for test case 1

Property	Test case 1
Length L (cm)	3.0
Initial porosity ϕ_0	0.113
Final porosity ϕ_f	0.274
Initial permeability K_0 (m^2)	2.6×10^{-18}
Final permeability K_f (m^2)	2.19×10^{-16}
Initial solid bulk density $\rho_{s,0}$ (kg/m^3)	1,810
Solid specific heat capacity γ_s (kJ/kg K)	2.0
Solid thermal conductivity κ_s (W/m K)	1.2
Mass decomposition m_f/m_0	0.795
Activation energy E_a (kJ/kmol)	2.6×10^5
Pre-exponential factor A (1/s)	1.14×10^{-18}, $m/m_0 \geq 0.91$ 1.84×10^{15}, $0.91 \geq m/m_0 \geq 0.795$
Order of reaction n	17.33, $m/m_0 \geq 0.91$ 6.3, $0.91 \geq m/m_0 \geq 0.795$
Heat of decomposition Δh_r (kJ/kg)	234.0
Gas molecular weight M_g (kg/kmol)	18.35
Gas initial viscosity $\mu_{g,0}$ (Pa s)	1.54×10^{-5}
Gas viscosity derivative $\frac{\partial \mu_{g,0}}{\partial T}$ (Pa s/K)	2.5×10^{-8}
Gas specific heat capacity γ_g (kJ/kg K)	3.0
Gas thermal conductivity κ_g (W/m K)	0.1
Initial pressure P_0 (Pa)	10^5
Initial temperature T_0 (°C)	24
Emissivity ϵ	0.85
Incident heat flux $q_i = \epsilon\sigma T_i^4$ (W/m^2)	2.8×10^5

Figure 2 compares our simulated predictions of the temperature, pressure and solid mass profiles with those obtained experimentally and numerically by Henderson and Wiecek [13]. In Henderson's numerical simulation, the solid elongation was not neglected. Thus, the control volume widths were not constant and their spatial positions changed during the simulation. To compare the numerical results with ours, we plot the temperature evolution for different initial position x_0 (Fig. 2a). As discussed before, the values of the heat capacity and thermal conductivity of the solid and gas have been chosen so that the temperature profiles are similar. We observe that this, nonetheless,

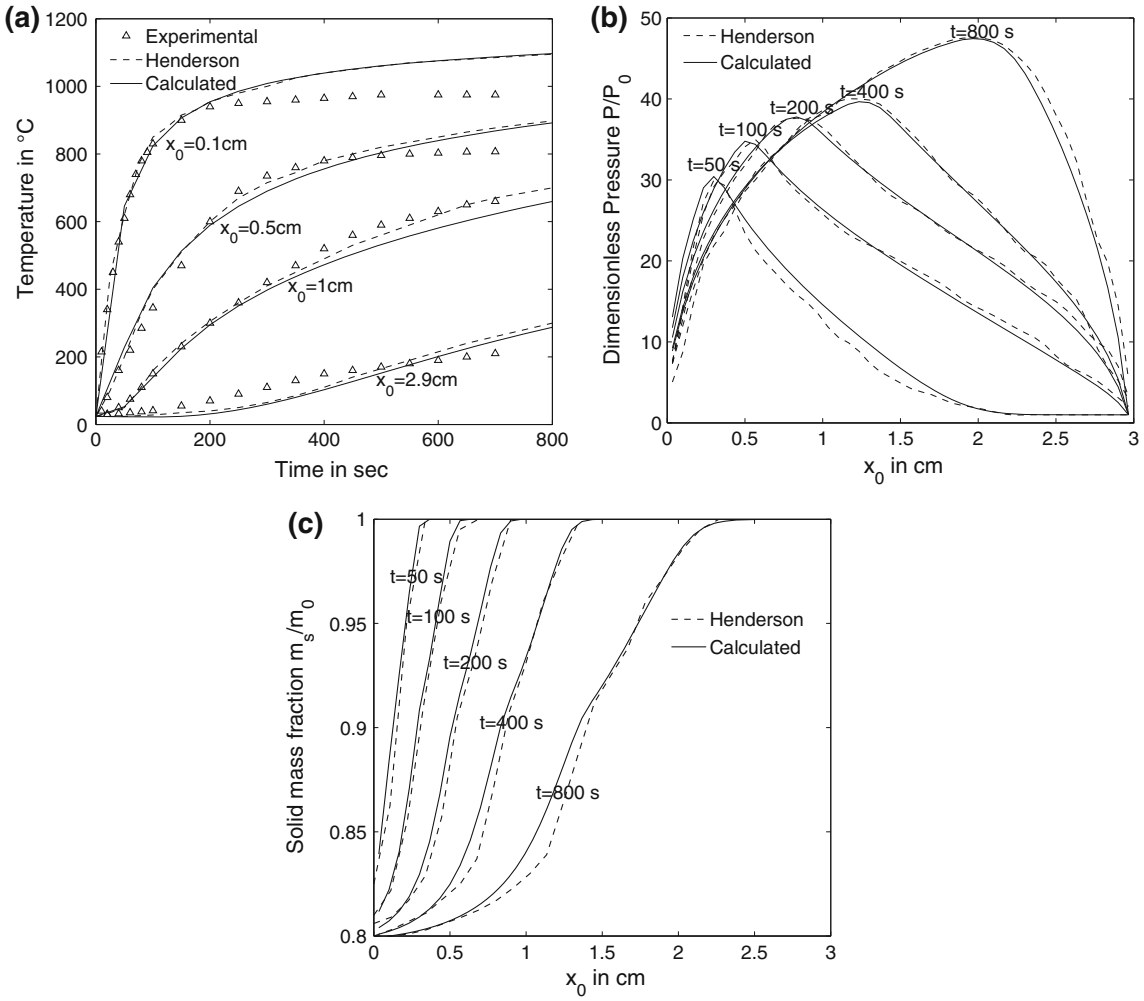

Fig. 2 **a** Temperature evolution for various initial positions, **b** pressure profile in the domain at various times and **c** solid mass fraction profile in the domain at various times. We observe good agreement between our numerical results and Henderson and Wieceks's experimental and numerical simulation results

results in similar profiles for the dimensionless pressure and the solid mass fraction (Fig. 2b, c). The relative error between our results and the numerical results of Henderson and Wiecek is <5 % while the relative error for the temperature between the experimental result and our results is <10 %. We conclude that our simplified model was able to reproduce with good agreement the coupling between heat propagation, chemical reaction and gas flow for the test case and that our assumptions about the process are appropriate.

4 Identification of the dimensionless numbers

We use IA to determine the set of dimensionless numbers that fully describe our mathematical model. IA is a well known scaling method first described by Ruark [25]. It has previously been applied to various mathematical models including immiscible waterflooding in oil reservoirs [27], miscible displacements in heterogeneous permeable media [9] and miscible displacements in soil columns [28]. To the best of our knowledge, IA has not been applied to a system with the boundary conditions implemented here, where the input is not an injected velocity but a heat flux or a fixed temperature.

The procedure introduces two arbitrary scaling factors for each of the variables in the equations. These scaling factors are linear (affine) transformations from dimensional to dimensionless space. They are then grouped into dimensionless scaling groups. Finally, the values of the scaling factors are selected to minimize the number of groups. The details of the procedure are presented in "Appendix". As the IA method is based on the existing differential equations and boundary conditions, the grouping and elimination of translation factors is physically meaningful provided the equations are complete for the process we are modelling. An important step in the

Table 2 Summary of scaling groups

Name	Notation	Definition	Description
Damköhler number	D_K	$\frac{A\rho_s\gamma_s L^2}{\kappa_s}$	$\frac{\text{chemical reaction rate}}{\text{heat diffusion rate}}$
Arrhenius number	N_a	$\frac{E_a}{R\Delta T}$	$\frac{\text{activation energy}}{\text{potential energy}}$
Reduced reaction enthalpy	Δh_r^*	$\frac{\Delta h_r}{\gamma_s \Delta T}$	$\frac{\text{energy liberated}}{\text{energy stored}}$
Reduced initial temperature	T_0^*	$\frac{T_0}{\Delta T}$	
Mass decomposition fraction	Δm^*	$\frac{\rho_{s,0}-\rho_{s,f}}{\rho_{s,0}}$	$\frac{\text{solid mass decomposition}}{\text{solid initial mass}}$
Reduced final porosity	δ	$\frac{\phi_f}{\phi_0}$	
Reduced final permeability	ξ	$\frac{K_f}{K_0}$	
Lewis number	L_e	$\frac{\phi_0\mu_{g,0}\kappa_s}{K_0P_0\rho_s\gamma_s}$	$\frac{\text{heat diffusivity}}{\text{pressure diffusivity}}$
Reduced gas density	ρ_g^*	$\frac{\phi_0 M_g P_0}{\rho_{s,0}R\Delta T}$	
Reduced gas specific heat	γ_g^*	$\frac{\gamma_g}{\gamma_s}$	
Reduced gas viscosity derivative	$\Delta\mu_g^*$	$\frac{\partial\mu_g}{\partial T}\frac{\Delta T}{\mu_{g,0}}$	
Gas heat conductivity reduction factor	$\Delta\kappa_g^*$	$\frac{\phi_0(\kappa_g-\kappa_s)}{\kappa_s}$	
Reduced radiative heat loss	ϵ^*	$\frac{\epsilon_s\sigma\Delta T^3}{\kappa_s}$	$\frac{\text{radiative heat loss}}{\text{heat flux by conduction}}$
Reaction order	n		

method is the introduction of a reference time scale τ, which is chosen here to be the time taken for heat to be conducted across the system at initial conditions.

$$\tau = \frac{\rho_{s,0}\gamma_s L^2}{\kappa_s} \tag{18}$$

This implies that the dimensionless rate of heat transfer is set to unity at initial conditions (see "Appendix", Eq. 43). We made this choice as there is no natural time scale for mass flow in the systems of interest as there is zero flow initially; moreover, both the thermal degradation and the in situ upgrading problems are controlled by the rate of reaction, which in turn depends upon the temperature and thus the rate of heat transfer. It is therefore natural to compare the efficiency of these processes by comparing the time taken for heat to conduct at initial (low temperature) conditions.

By employing the method presented, we obtain a minimal form of the dimensionless groups [27]. The groups are summarized in Table 2 and the values of the scaling groups for test case 1 in Table 3.

The Lewis number obtained through our analysis is actually a thermal Lewis number. It represents the ratio of thermal diffusivity α and pressure diffusivity D_P [29].

$$L_e = \frac{\alpha}{D_P} = \frac{\phi_0\mu_{g,0}\kappa_s}{K_0P_0\rho_s\gamma_s} \tag{19}$$

The Lewis number can be use to calculate a Péclet heat transfer number [15] which is defined here as

$$P_e = \frac{\rho_g\gamma_g v_g L}{\kappa_s} \tag{20}$$

and describres the ratio of heat driven by convection to thermal diffusion. As no fluid is injected, the fluid velocity is generated by the pressure gradients induced by heating. Hence, the Péclet number is local and varies with the dimensionless pressure and temperature:

$$P_e = \frac{\gamma_g^*}{L_e}\rho_{gD}v_{gD} \tag{21}$$

where ρ_{gD} and v_{gD} are defined in "Appendix" (Eqs. 58, 59).

The Damköhler number characterises the ratio of the reaction rate and the heat diffusion rate at infinite temperature. The Damköhler number we define here is a variation of Damköhler's second number, representing the ratio of the reaction rate and the diffusion rate [15]. In our model, we use the heat diffusion rate.

We validated our set of dimensionless numbers by constructing another test case (test case 2, Table 4) with different solid properties to test case 1 but with parameter values such that the dimensionless groups given in Table 3 have the same values as for test case 1 and 2. Figure 3 shows that the dimensionless temperature and pressure are almost identical for the two test cases, as we would expect. The dimensionless pressure and temperature error between case 1 and 2 are smaller than 0.1 %. We conclude that our set of scaling groups works as expected. The dimensionless numbers define a scaling relationship between different values of the dimensional parameters.

5 Calculation of reaction temperature

The Arrhenius number quantifies the impact of temperature on the chemical reaction rate but it can be seen that there is no obvious way of determining how hot the system needs to be before the reaction becomes important. The temperature at which the reaction appears will depend upon the time scale considered. This is a natural consequence of the exponential nature of the Arrhenius law (Eq. 1). Nonetheless it would be very useful to know what this "reaction temperature" is for any given system.

One useful consequence of the choice of reference timescale for our dimensionless analysis is the possibility to define this "reaction temperature". We chose the time scale for thermal diffusion to be our reference time scale

Table 3 Value of dimensionless groups for test case 1 and 2

Groups	Value	Groups	Value
D_K $(m/m_0 \geq 0.91)$	3.14×10^{21}	n $(m/m_0 \geq 0.91)$	17.33
D_K $(0.91 \geq m/m_0 \geq 0.795)$	5.2×10^{18}	n $(0.91 \geq m/m_0 \geq 0.795)$	6.3
N_a	26.2	T_0^*	0.25
δ	2.42	ξ	43.8
Δm^*	0.205	ρ_g^*	1.16×10^{-5}
L_e	2.2	$\Delta \mu_g^*$	1.93
γ_g^*	1.5	Δh_r^*	0.098
$\Delta \kappa_g^*$	0.1036	ϵ^*	2.05

Table 4 Summary of parameters for test case 2

Property	Case 2
Length L (cm)	2
Initial porosity ϕ_0	0.164
Final porosity ϕ_f	0.397
Initial permeability K_0 (m^2)	5.0×10^{-18}
Final permeability K_f (m^2)	1.14×10^{-16}
Initial solid bulk density $\rho_{s,0}$ (kg/m^3)	1,500
Solid specific heat capacity γ_s (kJ/kg K)	1.8
Solid thermal conductivity κ_s (W/m K)	0.7
Mass decomposition m_f/m_0	0.795
Activation energy E_a (kJ/kmol)	2.48×10^5
Pre-exponential factor A (1/s)	2×10^5, $m/m_0 \geq 0.91$ 3.24×10^{15}, $0.91 \geq m/m_0 \geq 0.795$
Order of reaction n	17.33, $m/m_0 \geq 0.91$ 6.3, $0.91 \geq m/m_0 \geq 0.795$
Heat of decomposition Δh_r (kJ/kg)	200
Gas molecular weight M_g (kg/kmol)	20
Gas initial viscosity $\mu_{g,0}$ (Pa s)	1.3×10^{-5}
Gas viscosity derivative $\frac{\partial \mu_{g,0}}{\partial T}$ (Pa s/K)	2.23×10^{-8}
Gas specific heat capacity γ_g (kJ/kg K)	2.7
Gas thermal conductivity κ_g (W/m K)	0.26
Initial pressure P_0 (Pa)	5×10^4
Initial temperature T_0 (°C)	10
Emissivity ϵ	0.86
Incident heat flux q_i (W/m^2)	2.3×10^5

(Eq. 18). The dimensionless reaction rate can be defined in terms of the Damköhler number, the Arrhenius number and the reduced initial temperature as

$$D_K \exp\left(-N_a\left(\frac{1}{T_D + T_0^*}\right)\right) = \frac{\text{time scale thermal diffusion}}{\text{time scale chemical reaction}} \tag{22}$$

where the dimensionless temperature T_D is defined as

$$T_D = \frac{T}{\Delta T}$$
$$\Delta T = T_i - T_0 \tag{23}$$

The Damköhler number represents the dimensionless reaction rate at a hypothetical infinite temperature and the exponential term represents an energy barrier to the reaction. This energy barrier is associated with a barrier or threshold temperature defined as:

$$T_B = \frac{E_a}{R} = N_a \Delta T \tag{24}$$

Thus the dimensionless reaction rate at the initial temperature T_0 is defined by the Damköhler number and the ratio of the threshold temperature to the initial temperature:

$$\frac{T_B}{T_0} = \frac{N_a}{T_0^*} \tag{25}$$

Similarly the dimensionless reaction rate at the applied (incident) temperature T_i is defined by the Damköhler number and the ratio of the threshold temperature to the incident temperature:

$$\frac{T_B}{T_i} = \frac{N_a}{1 + T_0^*} \tag{26}$$

As noted in our discussion of dimensionless time, for both of the applications examined here we are interested in evaluating how the reaction rate increases when the system is heated, because the reaction rate is insignificant at initial conditions. As the temperature increase in the domain, the reaction rate grows faster. We arbitrary chose 0.1 to be the limit when the reaction becomes significant.

$$D_K \exp\left(-\frac{N_a}{T_D + T_0^*}\right) \geq 0.1 \tag{27}$$

We can therefore calculate a threshold temperature from the the Arrhenius and Damkohler numbers as

$$T_R = \Delta T \frac{Na}{\log(10 D_K)} \tag{28}$$

For test case 1, we obtain a reaction temperature $T_R = 331$ °C. Figure 4a shows the solid mass profile for

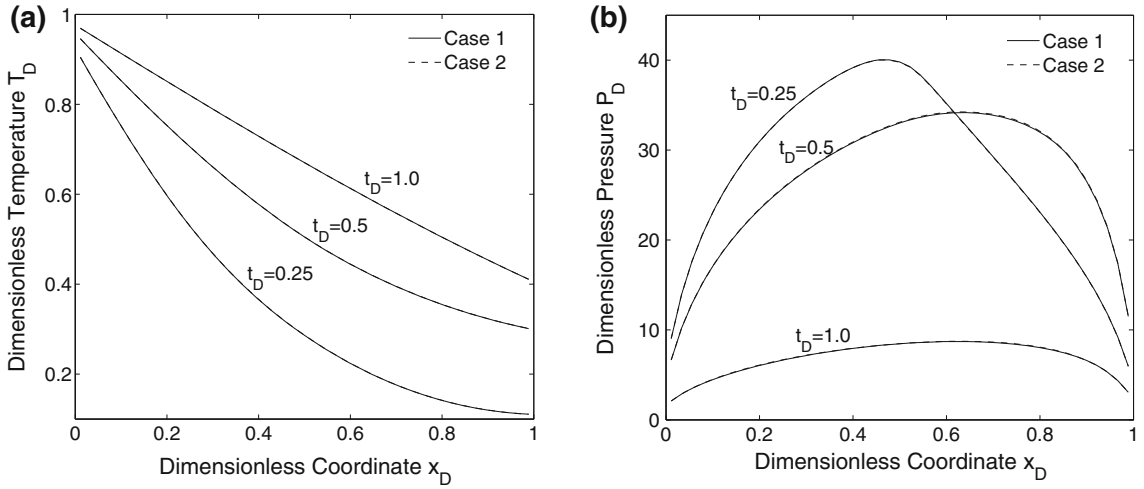

Fig. 3 Comparison of numerical results for **a** dimensionless temperature and **b** dimensionless pressure profiles at various times for test case 1 and 2. We observe that the numerical results are identical

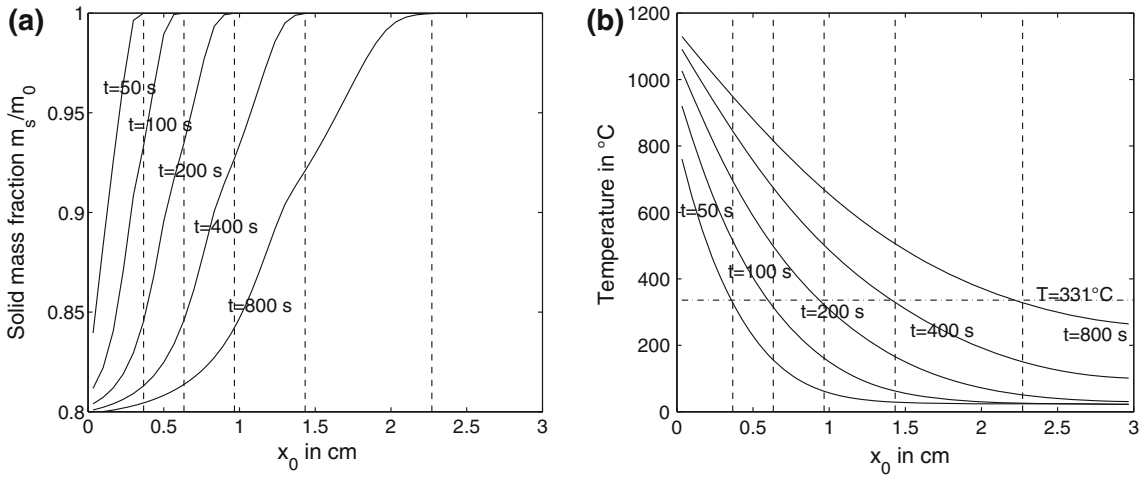

Fig. 4 Comparison of predicted and observed reaction temperature for test case 1. **a** In *plain line* the solid mass fraction profile at various times and in *dashed line* the position where the reaction appears. This position is then reported on **b** which shows the temperature profile at various times and compares the results with the predicted temperature $T_r = 331$ °C. We observe good agreement between the numerical and the predicted results

test case 1 at different times. The dashed lines indicate the position at which the reaction appears. We report these positions on the temperature profiles (Fig. 4b). Thus, the intersection between the dashed lines and the temperature profiles shows the temperature at the position where the chemical reaction appears. We observe that there is very good agreement between the reaction temperature calculated (Eq. 28) and the one observed. This validates our choice of 0.1 for our limit of significance. When the chemical reaction is more than 10 time slower than the heat conduction, it is too slow to be significant. When the dimensionless reaction rate is between 0.1 and 1, the change in solid mass fraction will start to decrease significantly over time.

6 Sensitivity analysis with experimental design

Some of the mechanisms that are involved in our model can be influenced by several non-dimensional parameters. For example, the chemical reaction is defined by the Damköhler number, the Arrhenius number and the reduced initial temperature. Moreover, one dimensionless number can impact several physical mechanisms. For example, the reduced initial temperature influences the chemical reaction and the radiative part of the boundary conditions, and the reduced gas specific heat capacity impacts heat accumulation in the fluid and heat flow by convection.

We used experimental design to investigate the sensitivity of the two processes of interest to the different

dimensionless numbers in order to determine which are the key dimensionless numbers in each case. This analysis also enables us to better understand the different factors that influence the performance in each case. The procedure for the sensitivity analysis is:

1. Choose the type of experimental design.
2. Determine a range for each parameter.
3. Choose the measure of system performance.
4. Perform the experimental trials.
5. Calculate the main and interaction effects.
6. Determine which parameters are important in characterising system performance.

In this study, we applied for each experiment a first-order response surface model with interactions [22]:

$$y = \beta_0 + \sum \beta_i x_i + \sum_{i \neq j} \beta_{ij} x_i x_j \tag{29}$$

where y is the response analysed and x_i the factors of interest. The β_i terms are called main factor effects and the β_{ij} terms the two-factor interaction effects. We used a factorial experimental design and assumed high order effects were negligible. This is appropriate when the response surface is to be approximated over a relatively small range of the independent variables where the response has little curvature. However, even when the error is large, this model can still be used for identifying primary parameters [22].

Factorial designs are widely used in experiments involving a large number of factors [21]. A two-level factorial design is a design where each of the k factors of interest has only two levels (-1 and 1). Such a design has exactly 2^k experimental trials or runs. If higher orders are negligible, then information on the main effects and low-order interactions between the factors can be obtained by running a fraction of the full factorial design.

An important parameter of a fractional design is the resolution [22]. A design is of resolution R if no p-factor effect ($0 < p < R$) is aliased with another effect containing less than $R - p$ factors. A design of resolution V has no main effect or two-factor interaction aliased with any other main effect or two-factor interaction. In this study, we will use fractional factorial design of resolution V. Algorithms to generate a design of resolution V are described in Myers et al. [22]. The results of the sensitivity analysis depend only on the resolution of the design and not on the choice of the generators.

Note that we can use a higher order design such as a second-order model. This design is similar to the first-order response surface model with interactions except that it also contains second order terms β_{ii}. To evaluate the β_{ii}, we need to use a three-level factorial design where each of the k factors of interest has three levels (-1, 0 and 1). For this design, the analysis is more expensive in CPU time as we need to perform 3^k trials. In our study, we tried the two models without noticing any difference in terms of determining which parameters were primary and which were insignificant, so we have reported here the results for the first order model with interactions.

After determining a range for each parameter and performing the trials, we can calculate the impact of the various factors and identify the important and insignificant parameters. We will apply the methodology to the case of thermal decomposition of polymer composite and thermal conversion of oil shale.

6.1 Thermal decomposition of polymer composites

We first consider a thin slab of polymer material used as a thermal protection system for space-shuttle and rocket nozzle. The performance of the thermal protection system is measured by the temperature in the protected area, on the right end of the domain (Fig. 1a), and by the amount of mechanical stress within the system. Therefore, we will use two measures of performance: first, the dimensionless temperature on the right boundary of the domain; secondly, the maximum dimensionless pressure in the domain.

The system depends on fourteen dimensionless groups. We select a design of resolution V comprising $n = 2^8$ trials. The next task is to evaluate a range for each scaling group. Table 5 gives the ranges used in this study. These were chosen after an extensive literature study [2, 6, 13] and bracket the values reported in the literature. We note that there is a very large range for orders of reaction (1–50). Recent papers [8, 20] tend to quote orders of 1 but older papers [6, 13] quote much larger values. This may be due to improvements in experimental techniques and analysis over time, but it is beyond the scope of this paper to explore further these issues.

In reality, data for properties such as molecular mass, heat capacity and viscosity of the gas or activation energy and order of the reaction are not independent, but in this experiment they are assumed to be for the purpose of the sensitivity analysis. Dependencies between parameters should be explored in future work as this may reduce the set of primary numbers further. Assuming they are independent, we obtain a range for our 14 dimensionless groups (Table 6).

The next step is to perform the experimental trials. We use our Matlab simulator introduced earlier and obtain the dimensionless temperature for every run. We then compute the main effects β_i and the interaction effects β_{ij} using the least squares method [22]. In order to obtain a normalized measure of the impact, we compute the t value

Table 5 Range of values for the various dimensional parameters of the thermal decomposition of polymer composite model

Property	Min.	Max.	Property	Min.	Max.
L (cm)	1	10	ϕ_0	0.05	0.15
ϕ_f/ϕ_0	2	4	K_0/ϕ_0 (m^2)	10^{-17}	10^{-14}
K_f/K_0	40	800	ρ_s (kg/m^3)	1,500	2,000
γ_s (kJ/kg K)	0.5	2	κ_s (W/m K)	0.5	2
m_f/m_0	0.6	0.96	E_a (kJ/kmol)	2×10^5	3×10^5
A (1/s)	10^{15}	10^{19}	n	1	50
Δh_r (kJ/kg)	100	1,000	M_g (kg/kmol)	16	30
μ_{g0} (Pa s)	10^{-15}	2×10^{-15}	$\frac{\partial \mu_g}{\partial T}$ (Pa s/K)	10^{-8}	3×10^{-8}
γ_g (kJ/kg K)	2	4	κ_g (W/m K)	0.05	0.2
P_0 (Pa)	10^5	10^6	T_0 (°C)	10	50
ϵ	0.6	0.9	T_i (°C)	1,000	1,600

Table 6 Range of values obtained for the various scaling groups for thermal decomposition of polymer composite range

Groups	Min.	Max.
D_K	3.75×10^{16}	8.00×10^{23}
N_a	15.1	38.0
T_0^*	0.18	0.340
δ	2	4
ξ	40	800
Δm^*	0.04	0.40
ρ_g^*	3.0×10^{-6}	3.80×10^{-4}
L_e	1.25×10^{-4}	50
$\Delta \mu_g^*$	0.475	4.77
γ_g^*	1	8
Δh_r^*	0.031	2.1
$\Delta \kappa_g$	0.03	0.15
ϵ^*	0.15	41.0
n	1	50

We observe that several numbers, such as L_e, vary over a large range, whereas other numbers, such as T_0^* vary over a much smaller

of each effect, which is simply the numerical effect divided by its associated standard error [14]. Figure 5a shows the t value of the main effects and Figure 5b shows the t value of the 12 most important interaction effects. The model consists of a total of $p = 105$ effects (main and interaction). In order to classify the importance of the effects, we define two measures of significance. The first measure compares the t-value of the effect with the critical value $t_{\alpha,d}$ of a student t-distribution with d degrees of freedom and a confidence limit $1 - \alpha$. Student distributions are generally used when estimating confidence intervals for normally distributed statistics where standard deviation is unknown [22]. In our case, for a confidence interval of 95 %, we compute the student distribution critical value with degree of freedom $d = 2^8 - p - 1 = 150$. We apply the Bonferroni correction [1] which takes the number of estimated effects into account by dividing it into the desired probability for the risk value α. We obtain the Bonferroni corrected t value referred as the t-limit:

$$t = t_{0.05/255,150} = 3.8 \tag{30}$$

The second measure referred as the l-limit is defined by the t value of Lenth's margin of error LME [19] based on a simple formula for the standard error of the effect:

$$l = LME \times t_{0.05,255} = 1.32 \times 1.97 = 2.6 \tag{31}$$

Effects that are smaller than the l-limit are considered to be insignificant (in white in Fig. 5). Effects that are greater than the t-limit are considered to be primary (in black in Fig. 5).

We observe that the factors are naturally regrouped into three classes:

- *The primary factors* ϵ^*, N_a, T_0^*, Δh_r^*, $\Delta \kappa_g^*$ and Δm^*. These are the factors which have their main effect or at least one of their interaction effects greater than the t-limit. The thermal protection system of the polymer composite depends mainly on these six factors and their interactions.
- *The secondary factors* γ_g^*, n, δ and D_K. These are the factors which have no main effect or any interaction effect greater than the t-limit but their main effect or at least one of their interaction effects is greater than the l-limit. The effect of the secondary factors is not negligible, but it is reduced compared to the effect of the primary factors.
- *The insignificant factors* $\Delta \mu_g^*$, ξ, ρ_g^* and L_e. These are the factors which have no main effect or interaction effect greater than the l-limit.

It is not surprising that the scaling groups ϵ^* and T_0^* are primary factors because they characterise the incident heat flux and the heat radiated (Eq. 15). Similarly, we would expect the Arrhenius number N_a and the reduced reaction enthalpy Δh_r^* to be primary factors as they describe the chemical reaction and its interaction with heat transfer as some of the heat conducted through the material is consumed by the endothermic reaction. The thermal protection system is more efficient for high Δh_r^* and low N_a, as high Arrhenius numbers delay the reaction.

It is more surprising that the Damköhler number is not one of the primary factors in our case. This is because of

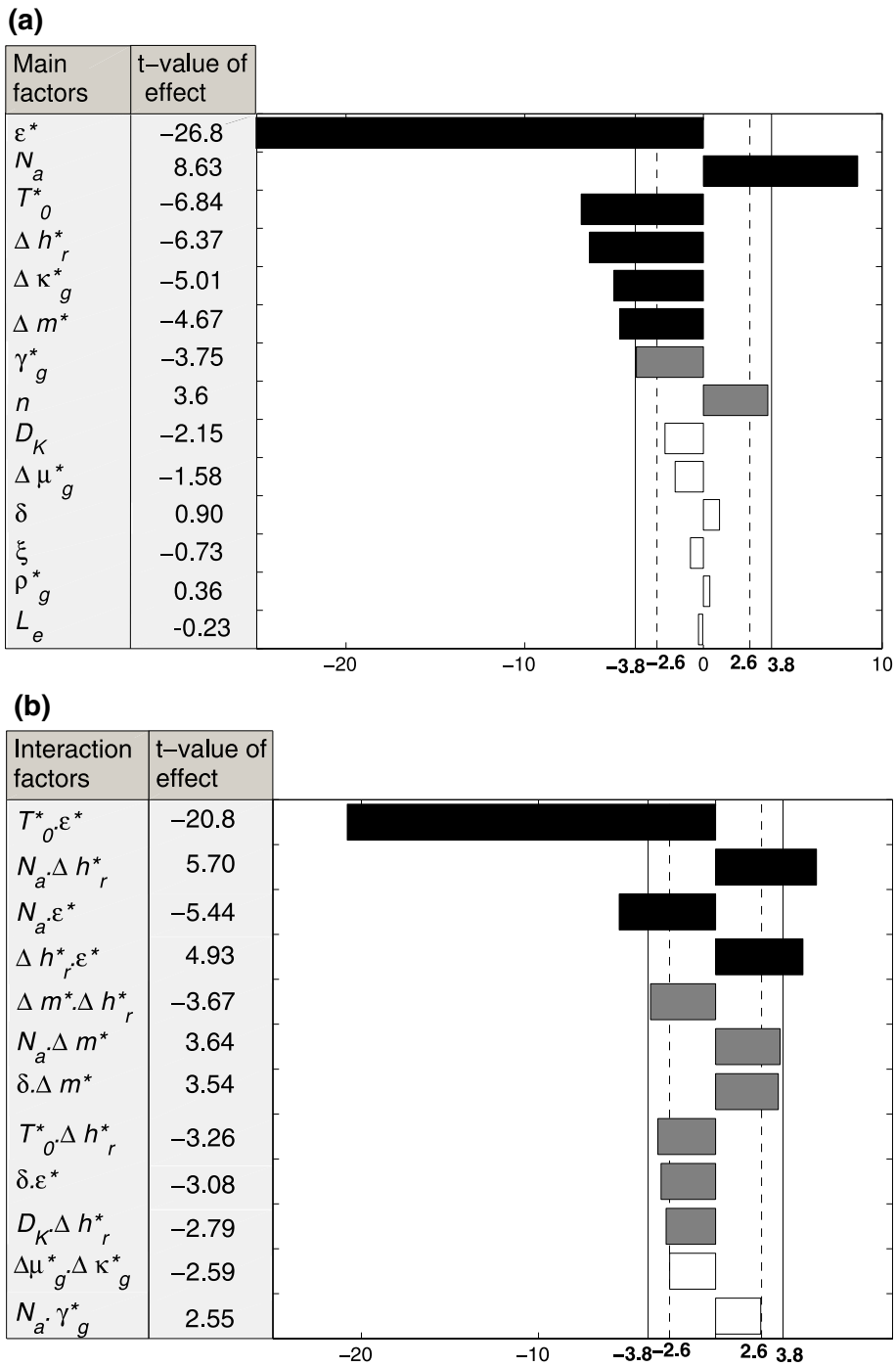

Fig. 5 Variability of thermal protection of polymer composite. The various effects are compared with Bonferroni *t*-limit (in *plain line*) and Lenth's margin of error l (in *dashed line*). Primary effects are represented in *black*, secondary in *grey* and insignificant in *white*

the wide range of temperature variation in this process which means that the Arrhenius number has more impact than the Damköhler number. The Lewis number is also insignificant. More generally, we observe that the scaling groups representing convection ($\Delta\mu_g^*$, ξ, and L_e) are insignificant. This is because the chemical reaction happens in an immobile phase. We conclude that heat convection has an insignificant impact on the thermal protection system.

Next, we perform the analysis using the maximum pressure in the domain between dimensionless time 0 and 1 as a measure of the system performance (instead of the right boundary dimensionless temperature). Figure 6a shows the t value of the main effects and Fig. 6b shows the t value of the 12 most important interaction effects. We obtain the critical values $t = 3.8$ and $l = 1.9$. In this case, we find that the primary factors are L_e, ρ_g^*, ξ, Δm^* and ϵ^* and the insignificant factors are $\Delta\kappa_g^*$ and Δh_r^*. The reduced gas density ρ_g^*

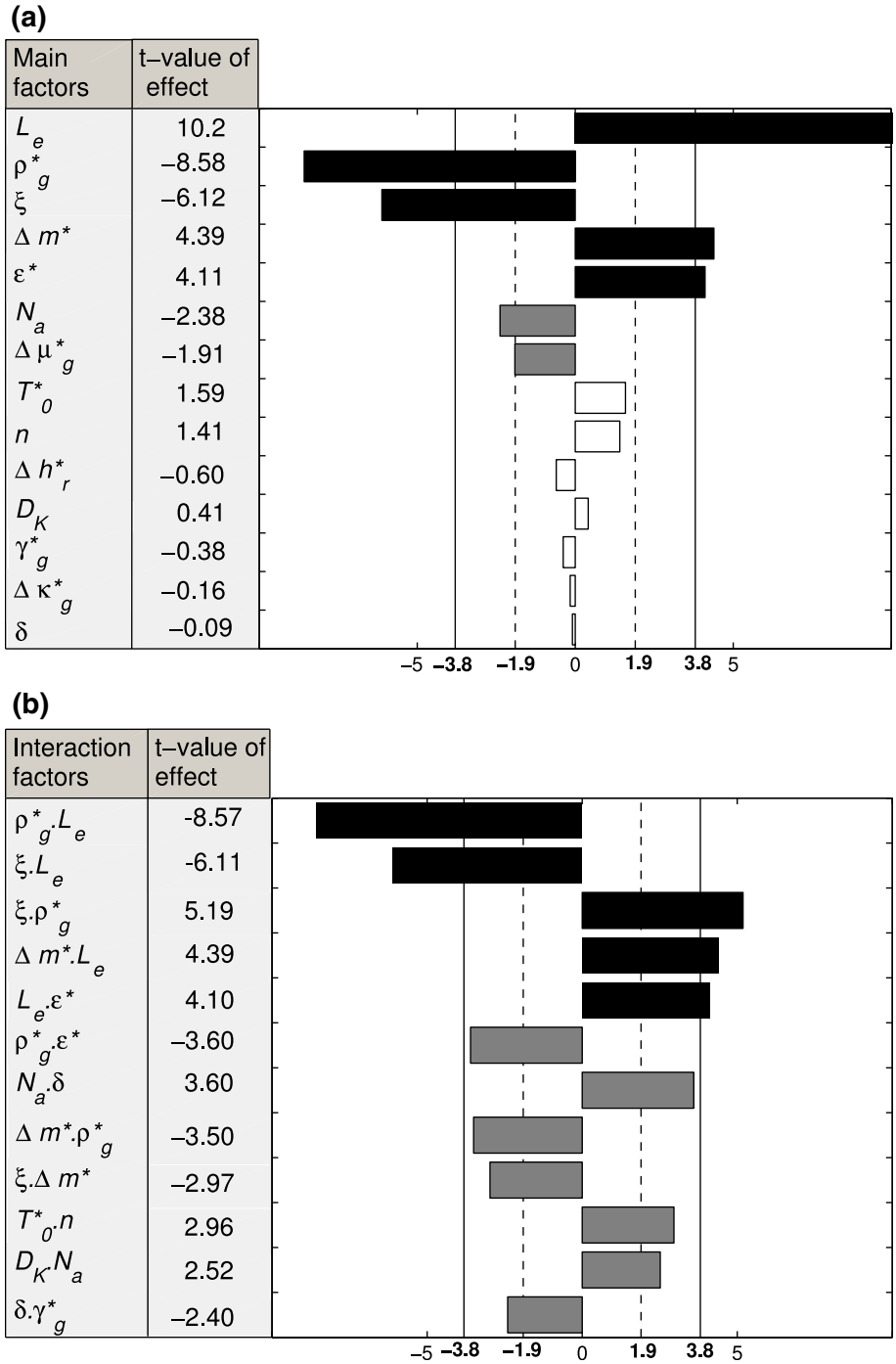

Fig. 6 Variability of maximum dimensionless pressure for polymer composite. The various effects are compared with Bonferroni *t*-limit (in *plain line*) and Lenth's margin of error *l* (in *dashed line*). Primary effects are represented in *black*, secondary in *grey* and insignificant in *white*

represents the ratio of the density of the gas product of the reaction and the density of the solid reactant. The smaller it is, the higher the volume of fluid created by the chemical reaction, and the higher the impact on the mechanical stress. The mass decomposition fraction Δm^* represents the quantity of solid reactant. For Δm^* closer to 1, more gas is generated and so more mechanical stress is applied to the domain. The Lewis number L_e quantifies the ratio of the heat diffusivity and pressure diffusivity. For large L_e, the pressure diffuses slowly and the mechanical stress is large. For large reduced final permeability ξ the pores have become larger due to the chemical reaction reducing the amount of the polymer matrix and so the pressure increase is less. Finally, the radiation number ϵ^* quantifies the incident heat flux and the heat loss. For large ϵ^*, the temperature increases more quickly within the system and so the rate of the chemical reaction also increases. Meanwhile the pressure diffusivity is unchanged. As a result, the mechanical stress increases.

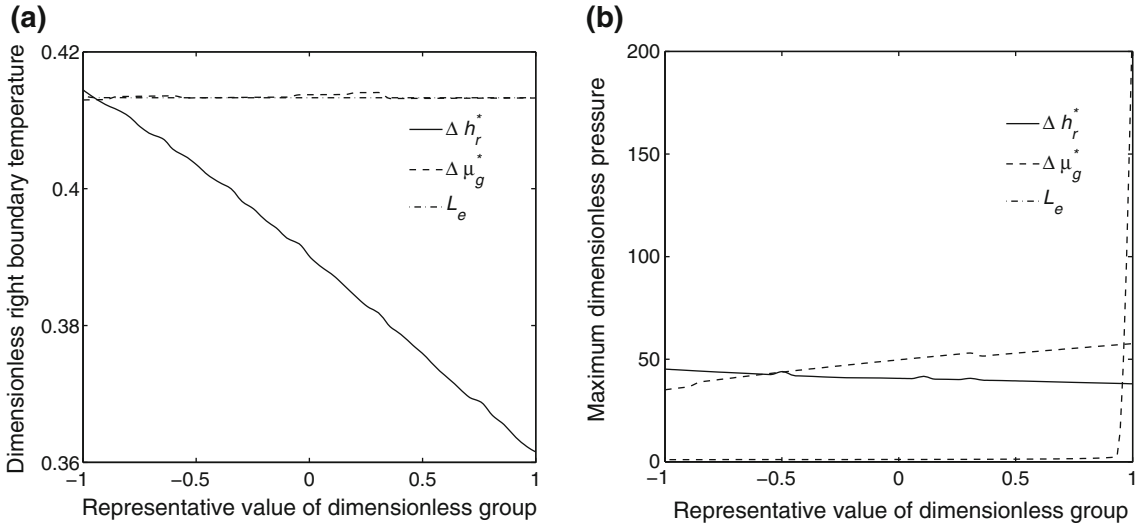

Fig. 7 Evolution of **a** dimensionless right boundary temperature and **b** maximum dimensionless pressure with respect to Δh_r^*, $\Delta \mu_g^*$ and L_e for thermal decomposition of polymer composite. The value of the dimensionless groups have been scaled so that -1 represents the minimum value and 1 the maximum value of each number according to Table 6

Our observations for both analyses are verified by comparing the evolution of the dimensionless right boundary temperature and the maximum dimensionless pressure with respect to the scaling groups considered for test case 1. Figure 7 shows the evolution for the groups Δh_r^*, $\Delta \mu_g^*$ and L_e. The x-axis has been scaled so that -1 represents the minimum of the scaling groups and 1 the maximum.

We conclude that 4 out of the 14 dimensionless numbers, defined for this model by IA, are insignificant when considering the performance of a thermal protection system using a polymer composite. This result can be illustrated by comparing the outcome from test case 1 with the outcome from two test cases in which parameters have been varied so that only the values of these insignificant numbers have changed (Table 7). For test case 3, $\Delta \mu_g^*$, ξ, ρ_g^* are taken at their minimum value and L_e at its maximum value. For test case 4, $\Delta \mu_g^*$, ξ, ρ_g^* are taken at their maximum value and L_e at its minimum value. The impact of changing these insignificant numbers on the temperature profile at various dimensionless times is shown in Fig. 8a. It can be seen that there is no observable difference between the three test cases. In contrast, if we consider the dimensionless pressure in the system (Fig. 8b), we see that this varies significantly between the test cases. This validates our method for identifying the least significant dimensionless numbers but also shows that the ranking of the importance of the different dimensionless numbers will depend upon the measure used to quantify system performance.

6.2 Thermal conversion of oil shale into non-reactive gas

We also apply the same sensitivity analysis to the modelling of the thermal upgrading of oil shale. In this process we are interested in the energy return over investment (EROI) ratio. The EROI is defined by the ratio of the energy content of the produced hydrocarbons and the energy supplied by the heater. If we define E_c as the energy content of 1 kg of recovered gas, the EROI is given by:

$$\text{EROI} = E_c \frac{\int_0^t \left(\rho_g v_{g|x=L} dt \right)}{\int_0^t \kappa_s \frac{\partial T}{\partial x}|_{x=0} dt} \tag{32}$$

We express this in terms of our dimensionless groups and variables using IA (see "Appendix"). This gives:

$$\text{EROI} = \frac{E_c}{\gamma_s \Delta T} \frac{1}{L_e} \frac{\int_0^{t_D} \left(\rho_{gD} v_{gD|x_D=1} dt_D \right)}{\int_0^{t_D} \frac{\partial T_D}{\partial x_D}|_{x_D=0} dt_D} \tag{33}$$

Therefore, the EROI of the process depends upon one additional scaling group, which we call the reduced energy content of the gas, and is defined by:

$$E_c^* = \frac{E_c}{\gamma_s \Delta T} \tag{34}$$

In this model, there is no incident heat flux and no heat loss by radiation ($\epsilon^* = 0$). Moreover, we assume for consistency with previous work that the order of the decomposition reaction is always one [4, 8]. Thus, our model of

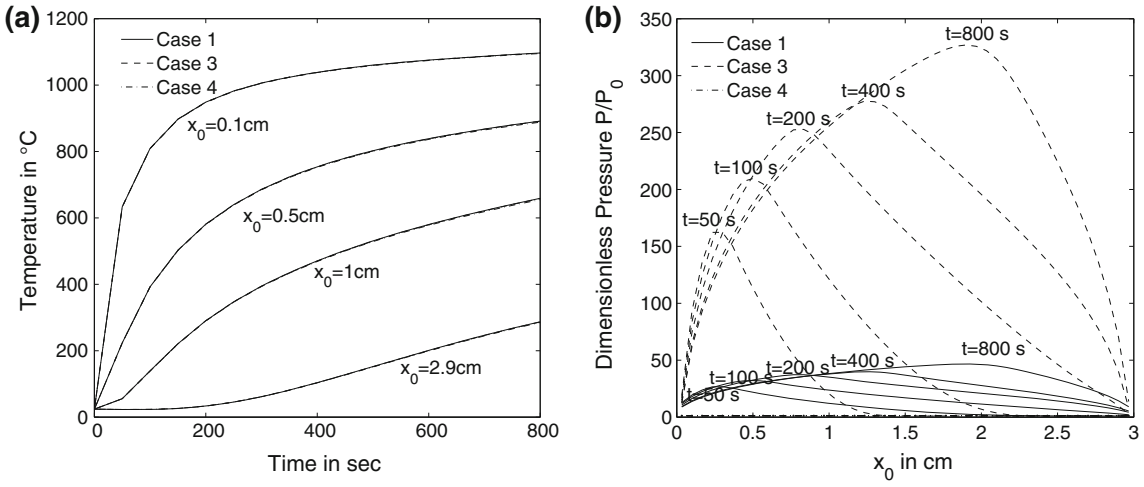

Fig. 8 Numerical simulation results for **a** temperature evolution for various initial positions and **b** pressure profile in the domain at various times. The temperature evolution is identical for the three test cases but the pressure profiles are different

Table 7 Value of dimensionless groups for test case 1, 3 and 4 (thermal decomposition of polymer composite)

Groups	Test case 1	Test case 3	Test case 4
D_K $(m/m_0 \geq 0.91)$	3.14×10^{21}	3.14×10^{21}	3.14×10^{21}
D_K $(0.91 \geq m/m_0 \geq 0.795)$	5.2×10^{18}	5.2×10^{18}	5.2×10^{18}
N_a	26.2	26.2	26.2
T_0^*	0.25	0.25	0.25
δ	2.42	2.42	2.42
ξ	43.8	43.8	43.8
Δm^*	0.205	0.205	0.205
ρ_g^*	1.16e−5	$\mathbf{3.0 \times 10^{-6}}$	$\mathbf{3.0 \times 10^{-5}}$
L_e	0.22	**50**	$\mathbf{1.25 \times 10^{-4}}$
$\Delta\mu_g^*$	1.93	**0.475**	**4.77**
γ_g^*	1.5	1.5	1.5
Δh_r^*	0.098	**0.031**	**2.1**
$\Delta\kappa_g$	0.1036	0.1036	0.1036
ϵ^*	2.05	2.05	2.05
Order $(m/m_0 \geq 0.91)$	17.33	17.33	17.33
Order $(0.91 \geq m/m_0 \geq 0.795)$	6.3	6.3	6.3

The numbers in bold are the ones that differs from test case 1

Table 8 Range of values for the various dimensional parameters of the thermal conversion of oil shale model

Property	Min.	Max.	Property	Min.	Max.
L (m)	1	3	ϕ_0	0.0001	0.0005
ϕ_f/ϕ_0	500	1,000	K_0/ϕ_0 (m^2)	10^{-13}	10^{-11}
K_f/K_0	1,000	10,000	ρ_s (kg/m^3)	1,500	2,000
γ_s (kJ/kg K)	0.5	2	κ_s (W/m K)	0.5	2
m_f/m_0	0.6	0.96	E_a (kJ/kmol)	1.50×10^5	2.5×10^5
A (1/s)	10^{11}	10^{13}	Δh_{r0} (kJ/kg)	100	1,000
M_g (kg/kmol)	16	50	μ_{g0} (Pa s)	10^{-5}	10^{-4}
$\frac{\partial\mu_g}{\partial T}$ (Pa s/K)	10^{-8}	3×10^{-8}	γ_g (kJ/kg K)	1	4
κ_g (W/m K)	0.01	0.2	T_i (°C)	300	400
P_0 (Pa)	10^5	10^6	T_0 (°C)	10	50
E_c (MJ/kg)	40	50			

thermal conversion of oil shale depends upon 13 dimensionless groups. As before we choose to use an experimental design of resolution V with $n = 2^8$ trials to evaluate the sensitivity of the EROI to these 13 different dimensionless numbers. The next task is to evaluate a range for each scaling group. Table 8 defines a minimum and maximum value for each dimensional parameter used to calculate each dimensionless number. These are determined from the literature [5, 30]. Table 9 gives the resulting ranges for the 13 dimensionless groups.

We observe several differences in the range of the dimensionless numbers compared with the thermal decomposition of polymer composite. The initial porosity and permeability of the solid are very small, but the ratio K_0/ϕ_0 is larger than in the polymer composite case. As a result, we obtain higher Lewis numbers. The porosity and permeability decomposition numbers δ and ξ are also larger

Table 9 Range of values obtained for the various scaling groups obtained for thermal conversion of oil shale model

Groups	Min.	Max.
D_K	3.75×10^{16}	7.2×10^{20}
N_a	46.3	120.3
T_0^*	0.73	1.29
δ	500	1,000
ξ	1,000	10,000
Δm^*	0.05	0.20
ρ_g^*	2.5×10^{-8}	8.0×10^{-6}
L_e	1.25×10^{-7}	0.027
$\Delta\mu_g^*$	0.025	1.17
γ_g^*	0.5	8.0
Δh_r^*	0.13	4.0
$\Delta\kappa_g$	6.0×10^{-5}	4.87×10^{-4}
E_c^*	51.3	480

We observe that several numbers, such as L_e, vary over a large range, whereas other numbers, such as T_0^* vary over a much smaller range

than in the polymer case. Another important difference is in the range of temperature ΔT (Eq. 23). The Arrhenius number N_a and the reduced initial temperature T_0^* are very high because the heating temperature T_i is smaller.

As before we perform the sensitivity analysis using the chosen experimental design and then compute the main and interaction effects using the least squares method [22]. Figure 9a shows the t value of the main effects and Fig. 9b shows the t value of the fifteen most important interaction effects. In this case the critical values are $t = 3.8$ and $l = 2.4$.

Thus, for the thermal decomposition of oil shale into non-reactive gas, the scaling groups are naturally regrouped into:

- *The primary factors* N_a, E_c, Δm^*, Δh_r^*, γ_g^* and ξ.
- *The secondary factors* D_k, δ, T_0^*.
- *The insignificant factors* $\Delta\kappa_g^*$, $\Delta\mu_g^*$, ρ_g^* and L_e.

We observe that, again, the Arrhenius number and the reduced reaction enthalpy are primary factors, the Damköhler number is a secondary factor and the Lewis number an insignificant parameter. For large reduced gas heat capacity γ_g^* the domain is heated by the advection of the gas and so the chemical reaction happens faster. Note that the reduced final permeability ξ is a primary factor in this study, whereas it was an insignificant factor in the thermal protection application for polymer composite. This may be due to the larger range for this parameter or to the measure of performance used (EROI instead of thermal protection).

We conclude that we can reduce the parameter space to 9 dimensionless numbers. As before, we illustrate this result by comparing 3 test cases with different values of the scaling groups (Table 10). Test case 5 has been built with values from Fan et al. [5]. Test cases 6 and 7 are derived from test case 5 with minimum or maximum values for the insignificant parameters $\Delta\kappa_g^*$, $\Delta\mu_g^*$, ρ_g^* and L_e. Test case 8 is the same as test case 5 apart from the value of the Arrhenius number, which takes a higher value (80) but still small enough to insure there is some reactions. Figure 10 shows the comparison of EROI for the four test cases. We see that the differences between the EROIs of test case 5 and test case 6, and test case 5 and test case 7 are smaller than 10 % while the difference in the EROI of test case 5 and test case 8 is higher than 90 %. This demonstrates that the impact of changes in one of the insignificant numbers on EROI is small compared with the impact of a change in one of the primary dimensionless numbers.

7 Conclusions

The main contribution of this paper is to apply IA, combined with sensitivity analysis using experimental design, to obtain a minimum number of dimensionless groups that characterise the problem of heat and mass flow in the presence of pyrolysis. We demonstrate that completely scaling a problem where solid decomposes into non-reactive gas with flexible boundary conditions requires the matching of fourteen dimensionless groups. These groups and their physical meaning are summarized in Table 2.

Several of the scaling groups obtained in our analysis have been identified in previous work, including the Damköhler and the Lewis number. They describe respectively the ratio of reaction rate and heat diffusion and the ratio of heat convection and heat diffusion. In our model however, the chemical reaction rate also depends on the Arrhenius number because of the temperature dependence of the reaction constant. By simple consideration of these dimensionless numbers, we were able to obtain a formula to predict the reaction temperature (Eq. 28).

The sensitivity analysis enabled us to divide the dimensionless numbers into three groups (primary, secondary and insignificant) based on the values of the t and l-limits. We applied the procedure to two systems of practical importance: thermal protection using polymer composite and thermal conversion of oil shale. In each case this classification helped us determine which physical mechanisms have a major impact on the efficiency of the process.

For the first application, the system performance is measured in terms of the temperature of the polymer on the far side of the domain (away from the heat source) and the pressure within the polymer (an indication of the mechanical stress). The lower the temperature, the better the heat protection; the lower the change in pressure, the less likely it is that the polymer will break up. We found that the temperature depends mainly on six factors: the

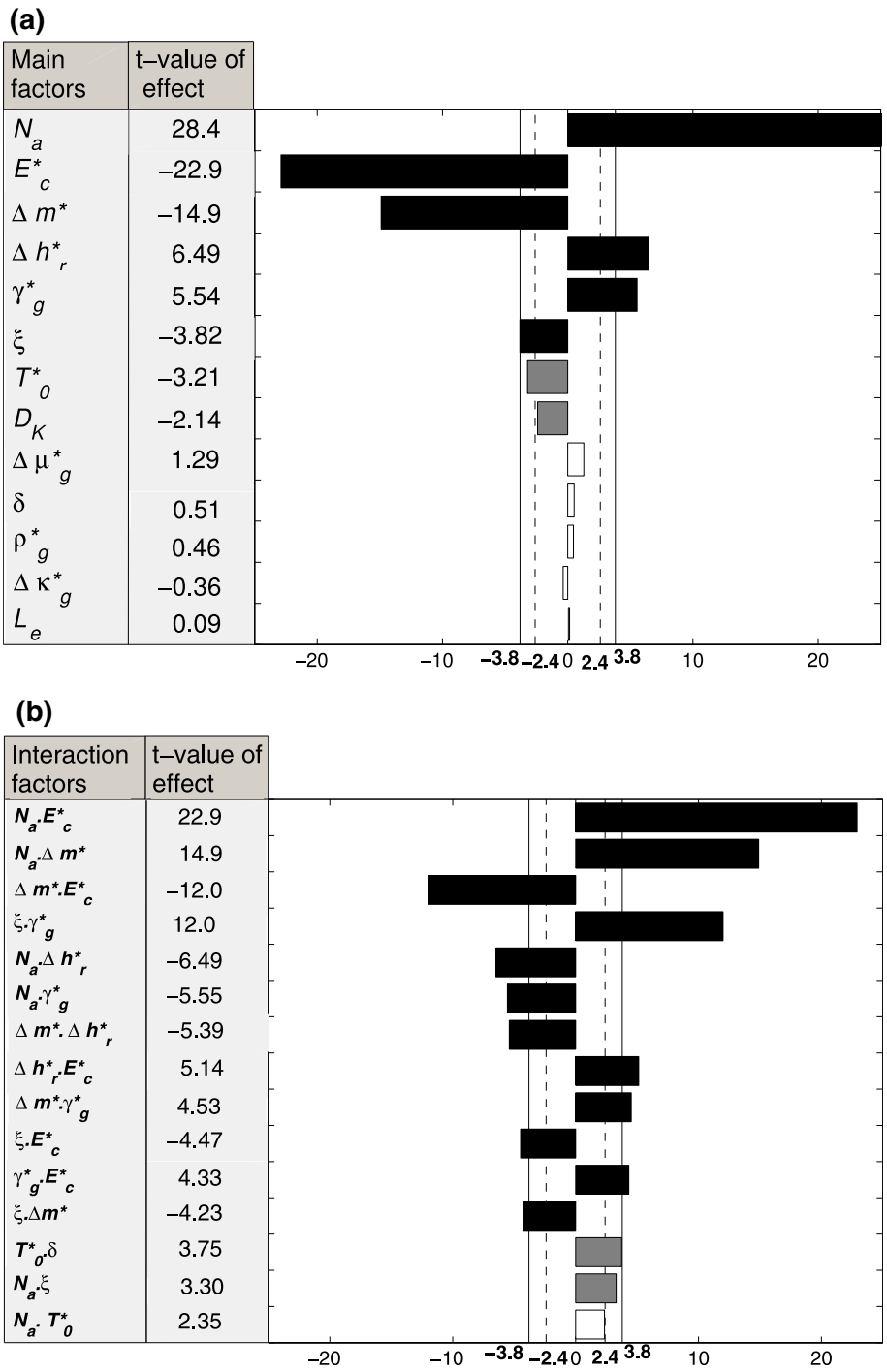

Fig. 9 Variability of EROI for thermal cracking of oil shale. The various effects are compared with Bonferroni *t*-limit (in *plain line*) and Lenth's margin or error (in *dashed line*). Primary effects are represented in *black*, secondary in *grey* and insignificant in *white*

radiation number, the Arrhenius number, the reduced initial temperature, the reduced reaction enthalpy, the gas thermal conductivity reduction factor and the mass decomposition number. These control the rate of polymer break down and the rate of heat transfer. The amount of mechanical stress depends mainly on the Lewis number, the reduced gas density, the reduced final permeability, the mass decomposition number and the radiation number.

For the second application the system performance is measured in terms of Energy Return on Investment (EROI). Obviously the higher this number the better the system performance. We observed that the EROI depends mainly on six primary factors: the Arrhenius number, the reduced energy content, the mass decomposition number, the reduced reaction enthalpy, the reduced gas specific heat capacity and the reduced final permeability. These numbers

Table 10 Value of dimensionless groups for test case 5, 6, 7 and 8

Groups	Test case 5	Test case 6	Test case 7	Test case 8
D_K	1.5×10^{19}	1.55×10^{19}	1.5×10^{19}	1.55×10^{19}
N_a	55.7	55.7	55.7	**80**
T_0^*	0.84	0.84	0.84	0.84
δ	1,000	1,000	1,000	1,000
ξ	3,000	3,000	3,000	3,000
Δm^*	0.15	0.15	0.15	0.15
ρ_g^*	1.85×10^{-6}	$\mathbf{2.55 \times 10^{-8}}$	$\mathbf{8.0 \times 10^{-6}}$	1.8×10^{-6}
L_e	2.8×10^{-5}	**0.027**	$\mathbf{1.25 \times 10^{-7}}$	2.8×10^{-5}
$\Delta\mu_g^*$	0.57	**0.0025**	**1.17**	0.57
γ_g^*	2.6	2.6	2.6	2.6
Δh_r^*	1.35	1.35	1.35	1.35
$\Delta\kappa_g$	3×10^{-4}	$\mathbf{6.0 \times 10^{-5}}$	$\mathbf{4.87 \times 10^{-4}}$	3×10^{-4}
E_c^*	123	123	123	123

The bold values are the ones that have been modified for the purpose of the test

control the amount of energy needed to obtain a useful product from the in situ upgrading.

For both applications, we observed that the Damköhler number, which describes the ratio of the reaction rate times the heat stored in the gas produced by the reaction to heat conduction through the solid was a secondary factor. This suggests that the rate of chemical reaction is mostly controlled by the energy barrier represented by the Arrhenius number.

The procedure applied to identify and rank the dimensionless number can be applied to other models and other applications. The model for thermal conversion of oil shale can be extended with a liquid phase to model more precisely the in situ upgrading of oil shale. The kerogen decomposes into liquid and gas, and the liquid experiences further decomposition into lighter products. The sensitivity analysis can help in reducing the number of experiments necessary to identify the behaviour of the system by only considering the most important parameters. It may also be useful when developing improved numerical models of these processes. For example, we could analyse the sensitivity of the number of non-linear iterations used to solve the conservation equations and try to reduce the number of significant parameters. This may also simplify the study of various non-linear solvers and the testing of their performance.

Acknowledgments The authors are grateful to Total E&P for funding this work. They would also like to thank the anonymous reviewers for their valuable comments and suggestions to improve the quality of the paper.

Appendix: Deriving the dimensionless groups by inspectional analysis

The general procedure of nondimensionalizing the equations that describe a physical process by inspectional analysis involves the introduction of arbitrary scaling factors. They make a linear transformation from dimensional to dimensionless space. The scaling factors are then grouped into dimensionless scaling groups, and their values are selected to minimize the number of groups.

We define the following linear transformations of every variables from the original dimensional space to a general dimensionless space:

$$\begin{aligned} &x = x_1^* x_D + x_2^* \quad t = t_1^* t_D + t_2^* \\ &\rho_s = \rho_{s1}^* \rho_{sD} + \rho_{s2}^* \\ &T = T_1^* T_D + T_2^* \quad P = P_1^* P_D + P_2^* \\ &v_g = v_1^* v_{gD} + v_2^* \quad q = q_1^* q_D + q_2^* \end{aligned} \tag{35}$$

In these transformations, the scale factors are the "*" quantities and the dimensionless variables are those with a subscript "D". There are 14 scale factors, two for each

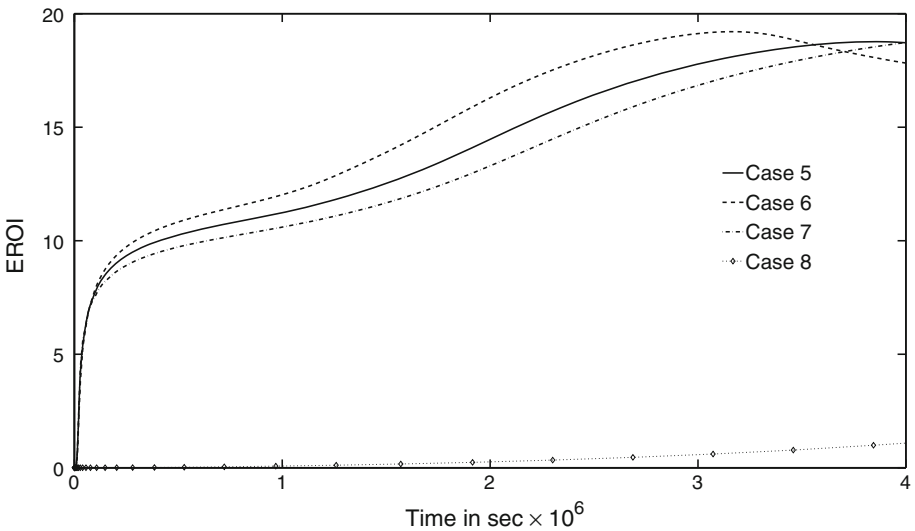

Fig. 10 Comparison of EROI for test case 5, 6, 7 and 8. We observe that the differences in the EROIs of test case 5 and test case 6, and test case 5 and test case 7 are smaller than 10 % while the difference in the EROI of test case 5 and test case 8 is higher than 90 %. Once again, we insist on the fact that the sensitivity analysis depends on the measure of performance used, here the EROI. Different conclusions may arise if using a different point of view

independent variable (x and t) and depend variable (ρ_s, T, P, v_g, q). The scale factors may be multiplicative (subscript 1) or additive (subscript 2). We substitute (35) into Eqs. (1), (7), (9), (13) and (14) and multiple by selected scale factors to make the equations dimensionless. We obtain:

- *Solid decomposition*

$$\underset{1}{\frac{\rho_{s1}^*}{\rho_{s,0}-\rho_{s,f}}}\frac{\partial \rho_{sD}}{\partial t_D} = \underset{2}{At_1^*}\left(\underset{1}{\frac{\rho_{s1}^*}{\rho_{s,0}-\rho_{s,f}}}\rho_{sD} + \underset{3}{\frac{\rho_{s2}^*-\rho_{s,f}}{\rho_{s,0}-\rho_{s,f}}}\right)^n \exp\left(-\underset{4}{\frac{E_a}{RT_1^*}}\frac{1}{T_D+\underset{5}{\frac{T_2^*}{T_1^*}}}\right) \tag{36}$$

$$\phi_D = 1 + \underset{6}{\frac{\phi_f-\phi_0}{\phi_0}}\left(1 - \underset{1}{\frac{\rho_{s1}^*}{\rho_{s,0}-\rho_{s,f}}}\rho_{sD} - \underset{3}{\frac{\rho_{s2}^*-\rho_{s,f}}{\rho_{s,0}-\rho_{s,f}}}\right) \tag{37}$$

$$K_D = 1 + \underset{7}{\frac{K_f-K_0}{K_0}}\left(1 - \underset{1}{\frac{\rho_{s1}^*}{\rho_{s,0}-\rho_{s,f}}}\rho_{sD} - \underset{3}{\frac{\rho_{s2}^*-\rho_{s,f}}{\rho_{s,0}-\rho_{s,f}}}\right) \tag{38}$$

- *Mass conservation*

$$\frac{\partial}{\partial t_D}\left(\phi_D\rho_{gD}\right) = -\underset{8}{\frac{v_1^*t_1^*}{\phi_0 x_1^*}}\frac{\partial}{\partial x_D}\left(\rho_{gD}\left(v_{gD}+\underset{9}{\frac{v_2^*}{v_1^*}}\right)\right) - \underset{10}{\frac{\rho_{s1}^*}{\rho_{s,0}}}\frac{\partial \rho_{sD}}{\partial t_D} \tag{39}$$

$$\rho_{gD} = \underset{11}{\frac{\phi_0 M_g P_1^*}{\rho_{s,0}RT_1^*}}\left(\frac{P_D+\frac{P_2^*}{P_1^*}}{T_D+\underset{5}{\frac{T_2^*}{T_1^*}}}\right)^{\boxed{12}} \tag{40}$$

- *Darcy's law*

$$v_{gD} = \underset{13}{\frac{K_0P_1^*}{\mu_{g,0}x_1^*v_1^*}}\frac{K_D}{\mu_{gD}}\frac{\partial P_D}{\partial x_D} - \underset{9}{\frac{v_2^*}{v_1^*}} \tag{41}$$

$$\mu_{gD} = 1 + \underset{14}{\frac{T_1^*}{\mu_{g,0}}}\frac{\partial \mu_g}{\partial T}\left(T_D - \underset{15}{\frac{T_0-T_2^*}{T_1^*}}\right) \tag{42}$$

- *Energy equation*

$$\left(\underset{10}{\frac{\rho_{s1}^*}{\rho_{s,0}}}m_D + \underset{16}{\frac{\rho_{s2}^*}{\rho_{s,0}}} + \phi_D\rho_{gD}\underset{17}{\frac{\gamma_g}{\gamma_s}}\right)\frac{\partial T_D}{\partial t_D} = -\underset{8}{\frac{v_1^*t_1^*}{\phi_0x_1^*}}\rho_{gD}\underset{17}{\frac{\gamma_g}{\gamma_s}}\left(v_{gD}+\underset{9}{\frac{v_2^*}{v_1^*}}\right)\frac{\partial T_D}{\partial x_D} - \underset{18}{\frac{q_1^*t_1^*}{\rho_{s,0}\gamma_s x_1^*T_1^*}}\frac{\partial q_D}{\partial x_D} - \underset{10}{\frac{m_1^*}{\rho_{s,0}}}\left(\underset{19}{\frac{\Delta h_{r,0}}{\gamma_sT_1^*}} + \underset{17}{\left(1-\frac{\gamma_g}{\gamma_s}\right)}\left(T_D - \underset{15}{\frac{T_0-T_2^*}{T_1^*}}\right)\right)\frac{\partial \rho_{sD}}{\partial t_D} \tag{43}$$

- *Fourier's law*

$$q_D = -\underset{20}{\frac{\kappa_sT_1^*}{q_1^*x_1^*}}\left(1+\phi_D\underset{21}{\frac{\phi_0\left(\kappa_g-\kappa_s\right)}{\kappa_s}}\right)\frac{\partial T_D}{\partial x_D} - \underset{22}{\frac{q_2^*}{q_1^*}} \tag{44}$$

- *Heat flow boundary conditions*

$$\begin{aligned}
&\text{at} \quad x_D = \underset{23}{-\frac{x_2^*}{x_1^*}} \quad \forall t_D \\
&q_D = \underset{24}{\frac{\epsilon_s\sigma T_1^{*4}}{q_1^*}}\left(\underset{25}{\frac{T_i^4}{T_1^{*4}}} - \underset{5}{\left(T_D+\frac{T_2^*}{T_1^*}\right)^4}\right) - \underset{22}{\frac{q_2^*}{q_1^*}} \\
&\text{or} \quad T_D = \underset{26}{\frac{T_i-T_2^*}{T_1^*}} \\
&\text{at} \quad x_D = \underset{27}{\frac{L-x_2^*}{x_1^*}} \quad \forall t_D \\
&q_D = -\underset{24}{\frac{\epsilon_s\sigma T_1^{*4}}{q_1^*}}\underset{5}{\left(T_D+\frac{T_2^*}{T_1^*}\right)^4} - \underset{22}{\frac{q_2^*}{q_1^*}} \\
&\text{or} \quad q_D = \underset{22}{-\frac{q_2^*}{q_1^*}}
\end{aligned} \tag{45}$$

- *Mass flow boundary conditions*

$$\begin{aligned}
&\text{at} \quad x_D = -\frac{x_2^*}{x_1^*} \quad \boxed{23} \quad \forall t_D \\
&P_D = \frac{P_0 - P_2^*}{P_1^*} \quad \boxed{28} \qquad \text{or} \qquad v_{gD} = -\frac{v_2^*}{v_1^*} \quad \boxed{9} \\
&\text{at} \quad x_D = \frac{L - x_2^*}{x_1^*} \quad \boxed{27} \quad \forall t_D \\
&P_D = \frac{P_0 - P_2^*}{P_1^*} \quad \boxed{28}
\end{aligned} \tag{46}$$

- *Initial conditions*

$$\begin{aligned}
&\rho_{sD} = \frac{\rho_{s,0} - \rho_{s2}^*}{\rho_{s1}^*} \quad \boxed{29} \\
&P_D = \frac{P_0 - P_2^*}{P_1^*} \quad \boxed{28} \ \text{at} \quad t_D = -\frac{t_2^*}{t_1^*} \quad \boxed{30} \quad \forall x_D \\
&T_D = \frac{T_0 - T_2^*}{T_1^*} \quad \boxed{15}
\end{aligned} \tag{47}$$

The scaling groups that appear in these equations are numbered (e.g., $\boxed{1}$). Each equation is dimensionless, and the 30 scaling groups are dimensionless too. The next task is to reduce the number of groups.

A large number of scaling groups can be set to zero by chosing the additive factors to be zero or to the initial or final value of the variable. Therefore, we choose:

$$\begin{aligned}
&x_2^* = 0 \quad t_2^* = 0 \\
&\rho_{s2}^* = \rho_{s,f} \\
&T_2^* = T_0 \quad P_2^* = 0 \\
&v_2^* = 0 \quad q_2^* = 0
\end{aligned} \tag{48}$$

Then, the groups 3, 9, 12, 15, 22, 23 and 30 are equal to zero. Next, we need to define the multiplicative factors. Setting scaling groups to one usually leaves the final formulation in a compact form that is generally free of constant. Therefore, we choose:

$$\begin{aligned}
&x_1^* = L \\
&\rho_{s1}^* = \rho_{s,0} - \rho_{s,f} \\
&T_1^* = \Delta T = T_1 - T_0 \quad P_1^* = P_0 \\
&v_1^* = \frac{K_0 P_0}{\mu_{g,0} L} \quad q_1^* = \kappa_s \frac{\Delta T}{L}
\end{aligned} \tag{49}$$

Thus, the groups 1, 13, 20, 26, 27, 28 and 29 are equal to one. For the multiplicative factor t_1^*, various time scales such as the time scale of the chemical reaction or the time scale of heat conduction could be chosen. Here we chose to normalize our time to the time taken for heat to diffuse at initial conditions. This has the advantage that group 18 in Eq. 45 is set to 1 i.e. the rate of change of heat transfer with distance is 1 at initial time.

$$t_1^* = \tau = \frac{\rho_{s,0} \gamma_s L^2}{\kappa_s} \Rightarrow \text{Group18} = 1 \tag{50}$$

Note that the order of the reaction n is an additional parameter. Therefore there remain 15 groups that are not yet defined. These remaining dimensionless groups are no longer arbitrary. They are:

$$\begin{aligned}
&D_2 = A\tau \quad D_4 = \frac{E_a}{R\Delta T} \quad D_5 = \frac{T_0}{\Delta T} \quad D_6 = \frac{\phi_f}{\phi_0} - 1 \\
&D_7 = \frac{K_f}{K_0} - 1 \quad D_8 = \frac{K_0 P_0 \tau}{\phi_0 \mu_{g0} L^2} \quad D_{10} = \frac{\rho_{s,0} - \rho_{s,f}}{\rho_{s,0}} \\
&D_{11} = \frac{\phi_0 P_0}{\rho_{s,0} \gamma_s R \Delta T} \\
&D_{14} = \frac{\Delta T}{\mu_{g,0}} \frac{\partial \mu_g}{\partial T} \quad D_{16} = \frac{\rho_{s,f}}{\rho_{s,0}} \quad D_{17} = \frac{\gamma_g}{\gamma_s} \quad D_{19} = \frac{\Delta h_{r,0}}{\gamma_s \Delta T} \\
&D_{21} = \frac{\phi_0 (\kappa_g - \kappa_s)}{\kappa_s} \quad D_{24} = \frac{\epsilon_s \sigma \Delta T^3 L}{\kappa_s} \quad D_{25} = \frac{T_i^4}{T_1^{*4}}
\end{aligned} \tag{51}$$

The last task is to minimise the number of groups by identifying dependent groups. We observe that:

$$\begin{aligned}
&D_{16} = 1 - D_{10} \\
&D_{25} = (1 + D_5)^4
\end{aligned} \tag{52}$$

Finally we obtain 13 groups. The system depends only on these groups and the order of reaction. The groups are:

$$\begin{aligned}
&D_K = A\tau \quad N_a = \frac{E_a}{R\Delta T} \quad T_0^* = \frac{T_0}{\Delta T} \quad \Delta m^* = \frac{\rho_{s,0} - \rho_{s,f}}{\rho_{s,0}} \\
&\delta = \frac{\phi_f}{\phi_0} \quad \xi = \frac{K_f}{K_0} \quad L_e = \frac{\phi_0 \mu_{g,0} L^2}{K_0 P_0 \tau} \quad \rho_g^* = \frac{\phi_0 M_g P_0}{\rho_{s,0} R \Delta T} \\
&\Delta \mu_g^* = \frac{\Delta T}{\mu_{g,0}} \frac{\partial \mu_g}{\partial T} \quad \Delta h_r^* = \frac{\Delta h_{r,0}}{\gamma_s \Delta T} \quad \gamma_g^* = \frac{\gamma_g}{\gamma_s} \quad \Delta \kappa_g^* = \frac{\phi_0 (\kappa_g - \kappa_s)}{\kappa_s} \\
&\epsilon^* = \frac{\epsilon_s \sigma \Delta T^3 L}{\kappa_s}
\end{aligned} \tag{53}$$

The dimensionless groups satisfy the scaling requirements for the one-dimensional problem. We can demonstrate that they are independent by using the method of elementary row operations descibed in [27]. We obtain the following form of the dimensionless equation:

- *Solid decomposition*

$$\frac{\partial \rho_{sD}}{\partial t_D} = D_K \rho_{sD}^n \exp\left(-\frac{N_a}{T_D + T_0^*}\right) \tag{54}$$

$$\phi_D = 1 + (1 - \delta)(1 - \rho_{sD}) \tag{55}$$

$$K_D = 1 + (1 - \xi)(1 - \rho_{sD}) \tag{56}$$

- *Mass conservation*

$$\frac{\partial}{\partial t_D}\left(\phi_D \rho_{gD}\right) = -\frac{1}{L_e}\frac{\partial}{\partial x_D}\left(\rho_{gD} v_{gD}\right) - \Delta m^* \frac{\partial \rho_{sD}}{\partial t_D} \tag{57}$$

$$\rho_{gD} = \rho_g^*\left(\frac{P_D}{T_D + T_0^*}\right) \tag{58}$$

- *Darcy's law*

$$v_{gD} = \frac{K_D}{\mu_{gD}}\frac{\partial P_D}{\partial x_D} \tag{59}$$

$$\mu_{gD} = 1 + \Delta\mu_g^*\left(T_D - T_0^*\right) \tag{60}$$

- *Energy equation*

$$\begin{aligned}&\left(1 - \Delta m^*(1 - \rho_{sD}) + \phi_D \rho_{gD}\gamma_g^*\right)\quad \frac{\partial T_D}{\partial t_D}\\ &= -\frac{1}{L_e}\rho_{gD}\gamma_g^* v_{gD}\frac{\partial T_D}{\partial x_D} - \frac{\partial q_D}{\partial x_D}\\ &\quad - \Delta m^*\left(\Delta h_r^* + \left(1 - \gamma_g^*\right)T_D\right)\frac{\partial \rho_{sD}}{\partial t_D}\end{aligned} \tag{61}$$

- *Fourier's law*

$$q_D = -\left(1 + \phi_D \Delta\kappa_g\right)\frac{\partial T_D}{\partial x_D} \tag{62}$$

- *Heat flow boundary conditions*

$$\begin{aligned}&\text{at}\quad x_D = 0\quad \forall t_D\\ &q_D = Q_i^* - \epsilon^*\left(T_D + T_0^*\right)^4\quad \text{or}\quad T_D = 1\\ &\text{at}\quad x_D = 1\quad \forall t_D\\ &q_D = -\epsilon^*\left(T_D + T_0^*\right)^4\quad \text{or}\quad T_D = 0\end{aligned} \tag{63}$$

- *Mass flow boundary conditions*

$$\begin{aligned}&\text{at}\quad x_D = 0\quad \forall t_D\\ &P_D = 0\quad \text{or}\quad v_{gD} = 0\\ &\text{at}\quad x_D = L\quad \forall t_D\\ &P_D = 0\quad \text{or}\quad v_{gD} = 0\end{aligned} \tag{64}$$

- *Initial conditions*

$$\begin{aligned}&\rho_{sD} = 1\\ &P_D = 1\quad \text{at}\quad t_D = 0\quad \forall x_D\\ &T_D = 0\end{aligned} \tag{65}$$

References

1. Anderson MJ, Whitcomb PJ (2007) DOE simplified: practical tools for effective experimentation, 2nd edn. Productivity Press, New York City
2. Bai Y, Vallee T, Keller T (2008) Modeling of thermal responses for FRP composites under elevated and high temperatures. Compos Sci Technol 68(1):47–56
3. Bennon WD, Incropera FP (1987) A continuum model for momentum, heat and species transport in binary solid–liquid phase cahnge systems—I. Model formulation. Int J Heat Mass Transf 30(10):2161–2170
4. Braun RL, Burnham AK (1990) Mathematical model of oil generation, degradation, and expulsion. Energy Fuels 4(2):132–146
5. Fan Y, Durlofsky L, Tchelepi H (2010) Numerical simulation of the in situ upgrading of oil shale. In: SPE reservoir simulation symposium, 2–4 February 2009, The Woodlands, TX, USA
6. Florio J, Henderson JB, Test FL, Hariharan R (1991) A study of the effects of the assumption of local-equilibrium on the overall thermally-induced response of decomposing, glass-filled polymer composite. Int J Heat Mass Transf 34(4):135–147
7. Fowler T, Vinegar H (2009) Oil shale ICP-Colorado field pilot. In: SPE western regional meeting, 24–26 March 2009, San Jose, CA, USA
8. Gersten J, Fainberg V, Hetsroni G, Shindler Y (1999) Kinetic study of the thermal decomposition of polypropylene, oil shale, and their mixture. Fuel 79(13):1679–1686
9. Gharbi RBC (2002) Dimensionally scaled miscible displacements in heterogeneous permeable media. Transp Porous Media 48(3):271–290
10. Henderson JB, Emmerich WD, Hagemann L, Post E (1993) Thermophysical property measurement on a complex high-temperature polymer composite. High Temp High Press 25(6):693–698
11. Henderson JB, Verma YP, Tant MR, Moore GR (1983) Measurement of the thermal conductivity of polymer composites to high temperatures using the line source technique. Polym Compos 4:219–224
12. Henderson JB, Wiebelt JA, Tant MR (1985) A model for the thermal response of polymer composite materials with experimental verification. J Compos Mater 19:579–595
13. Henderson JB, Wiecek TE (1988) A numerical study of the thermally-induced response of decomposing, expanding polymer composites. Wärme und Stoffübertragung 22(5):275–284
14. Hogg RT, McKean JW, Craig AT (2005) Introduction to mathematical statistics, 6th edn. Pearson Education, Upper Saddle River
15. Johnson RW (1998) The handbook of fluid dynamics. CRC Press, Boca Raton
16. Kansa EJ, Perler HE, Chaiken RF (1977) Mathematical model of wood pyrolysis including internal convection force. Combust Flame 29:311–324
17. Kelley CT (2003) Solving nonlinear equations with Newton's method. SIAM, Philadelphia
18. Kumar J, Fusetti L, Corre B (2011) Modeling in situ upgrading of extraheavy oils/tar sands by subsurface pyrolysis. In: Canadian unconventional resources conference, 15–17 November 2011, AB, Canada
19. Lenth R (1989) Quick and easy analysis of unreplicated factorials. Technometrics 31:469–473
20. Miller RS, Bellan J (1996) Analysis of reaction products and conversion time in the pyrolysis of cellulose and wood particles. Combust Sci Technol 119(1–6):331–373
21. Montgomery DC (2000) Design and analysis of experiments, 5th edn. Wiley, New York City
22. Myers RH, Montgomery DC, Anderson-Cook CM (2009) Response surface methodology: process and product optimization using design of experiments, 3rd edn. Wiley, Oxford
23. Patankar SV (1980) Numerical heat transfer and fluid flow. Hemisphere, New York
24. Puiroux N, Prat A, Quintard M (2004) Non-equilibrium theories for macroscale heat transfer: ablative composite layer systems. Int J Therm Sci 43(6):541–554

25. Ruark AE (1935) Inspectional analysis: a method which supplements dimensional analysis. J Elisha Mitchell 51:127–133
26. Ruzicka MC (2008) On dimensionless numbers. Chem Eng Res Des 86(8a):835–868
27. Shook M, Li D, Lake WL (1992) Scaling immiscible flow through permeable media by inspectional analysis. In Situ 16(4):311–349
28. Shukla MK, Kastanek FJ, Nielsen DR (2002) Inspectional analysis of convective-dispersive equation and application on measured breakthrough curves. Soil Sci Soc Am J 66(4):1087–1094
29. Staggs JEJ (2003) Heat and mass transport in developing chars. Polym Degrad Stab 82(2):297–307
30. Youstos MSK, Mastorakos E, Cant RS (2013) Numerical simulation of thermal and reaction front for oil shale upgrading. Chem Eng Sci 94:200–213
31. Yuen RKK, Yeoh GH, Davis GD, Leonardi E (2007) Modelling the pyrolysis of wet wood—I. Three-dimensional formulation and analysis. Int J Heat Mass Transf 50(21–22):4371–4386